




**Magnetic breakdown and chiral magnetic effect at Weyl-semimetal tunnel junctions**Adam Yanis Chaou , Vatsal Dwivedi , and Maxim Breitkreiz \**Dahlem Center for Complex Quantum Systems and Fachbereich Physik, Freie Universität Berlin, 14195 Berlin, Germany*

(Received 3 March 2023; revised 21 April 2023; accepted 8 June 2023; published 29 June 2023)

We investigate magnetotransport across an interface between two Weyl semimetals whose Weyl nodes project onto different interface momenta. Such an interface generically hosts Fermi arcs that connect Weyl nodes of identical chirality in different Weyl semimetals (homochiral connectivity)—in contrast to surface Fermi arcs that connect opposite-chirality Weyl nodes within the same Weyl semimetal (heterochiral connectivity). We show that electron transport along homochiral-connectivity Fermi arcs, in the presence of a longitudinal magnetic field, results in a universal longitudinal magnetoconductance of  $e^2/h$  per magnetic flux quantum. Furthermore, a weak tunnel coupling can result in a close encounter of two homochiral-connectivity Fermi arcs, enabling magnetic breakdown. Above the breakdown field the interface Fermi arc connectivity is effectively heterochiral, leading to a saturation of the conductance.

DOI: [10.1103/PhysRevB.107.L241109](https://doi.org/10.1103/PhysRevB.107.L241109)

**Introduction.** Weyl semimetals (WSMs) are a class of three-dimensional semimetals characterized by pairs of opposite-chirality Weyl fermions instantiated as topologically protected gapless points in the bulk Brillouin zone (BZ) [1–11]. Individual Weyl fermions exhibit the chiral anomaly [12,13]—a violation of particle-number conservation in the presence of parallel electric and magnetic fields. The chiral anomaly manifests as spectral flow on chiral zeroth Landau levels, which disperse either parallel or antiparallel to an applied magnetic field depending on the chirality of the Weyl fermions [14]. In a finite system, the reconnection of this spectral flow necessitates the existence of gapless Fermi-arc surface states, which connect Weyl nodes of opposite chirality.

One of the most striking transport phenomena associated with the chiral anomaly is the *chiral magnetic effect* (CME), which results in a positive longitudinal magnetoconductance [9,15,16]. In the ballistic (also called ultra-quantum) limit where transport is governed solely by the chiral lowest Landau level, the longitudinal conductance is predicted to show a universal linear dependence on the magnetic field [17]. Experimental evidence of the chiral anomaly by way of the CME has, however, turned out to be challenging because of various extrinsic effects [18,19]. Moreover, since the Weyl nodes often do not reside exactly at the Fermi energy, the ballistic-limit CME is only achieved at large nonuniversal field strengths.

In this paper, we show that in tunnel junctions between two WSMs both the CME and the Fermi arcs combine to give alternative magnetoconductance signatures of the chiral anomaly. We consider WSMs with Weyl nodes whose transverse momenta are displaced with respect to one another. Previous work has focused on the tunnel conductance across interfaces where the Fermi pockets of the two WSMs overlap [20–24]. We instead consider nonoverlapping Fermi pockets, which, in the absence of further ingredients, would simply result in a vanishing tunnel conductance. We, however, show

that upon adding a magnetic field normal to the interface, the chiral Landau levels can transmit across the interface via the interface Fermi arcs while higher Landau levels are reflected. In contrast to bulk realisations, the ballistic-limit CME across the tunnel junction (characterised by a universal, linear in field conductance) occurs around zero magnetic field irrespective of whether the Weyl nodes are at exactly the Fermi energy.

We further show that magnetotransport across the tunnel junction allows for the exploration of the phenomenon of *magnetic breakdown*—magnetic-field induced quantum tunneling between disjoint equienergy contours [25–28]. In bulk materials, level separation is typically too large for magnetic breakdown to manifest at realistic magnetic field strengths [27,29]. In a tunnel junction, however, the level repulsion between Fermi arcs can be made small by weakening the coupling [30] at the interface. The onset of magnetic breakdown causes an effective switch between topologically distinct Fermi-arc connectivities at the interface (see below), signified by a saturation of the magnetoconductance above a characteristic magnetic-breakdown field, which is controlled by the tunneling amplitude.

In the following, we begin by deriving the conductance from topological arguments. We then generalize the result so as to account for the possibility of magnetic breakdown. Finally, we confirm our predictions by numerical computations for a concrete lattice model for a WSM.

**Tunnel-junction CME.** We consider electron transport through a tunnel junction of two Weyl semimetals in the presence of a magnetic field of magnitude  $B$  normal to the interface. We assume that the projection onto the interface BZ of the Fermi surfaces of the Weyl nodes from different sides of the interface are separated by lattice momentum much larger than the inverse magnetic length  $l_B^{-1} = \sqrt{eB/\hbar}$ . This prevents direct scattering across the interface between the bulk Weyl nodes.

In the presence of the magnetic field, each Weyl node has an imbalance in the number of left and right movers because of the  $N(B)$ -fold degenerate chiral lowest Landau level where

\*breitkr@physik.fu-berlin.de

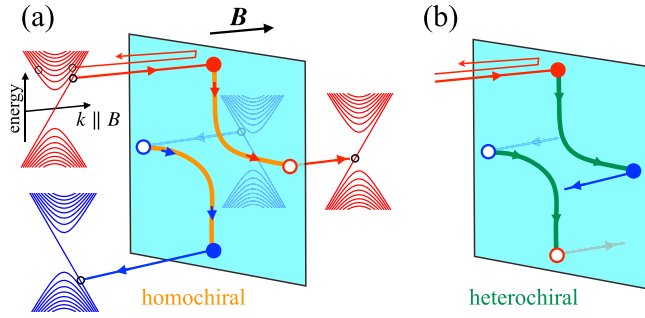


FIG. 1. Spectral flow at the interface between two Weyl semimetals with a longitudinal magnetic field. (a) Interface Fermi arcs with homochiral connectivity (orange lines) lead to a full transmission of the chiral zeroth Landau level across the interface (indicated by thick red/blue arrows going from/to the Landau-level spectrum) while the higher Landau levels are reflected. (b) Same as (a) but for heterochiral connectivity of Fermi arcs (green lines), in which case the chiral Landau levels are reflected.

$N(B)$  is the number of magnetic flux quanta through the interface [31]. As the surplus spectral flow from the chiral modes cannot terminate at the interface, there must exist a continuous chain of states (the interface Fermi arcs) that reconnects the interface projection of one Weyl node to that of another, as illustrated in Fig. 1. This follows from particle conservation and the observation that an infinitesimal field only couples states that are infinitesimally close in transverse momenta.

Consequently, two such types of Fermi arcs are possible—those that connect projections of opposite-chirality Weyl nodes in the same WSM and those which connect same-chirality nodes in WSMs on opposite sides of the interface [32–37]. We term the two connectivities *heterochiral* and *homochiral*, respectively. While the connectivity of the interface Fermi arcs is a topological property (see Supplemental Material, SM, for an alternative topological argument [38]), their shape is nonuniversal and depends on system details such as boundary potentials and the tunneling amplitude. The tunnel conductance, however, does not depend on the specific Fermi-arc shape but only on the topological connectivity and the presence/absence of close encounters of different Fermi arcs.

We first consider the situation without encounters, i.e., the interface Fermi arcs being separated by lattice momenta much larger than  $\ell_B^{-1}$ . In this case, a pair of homochiral Fermi arcs perfectly transmit the incoming mode across the interface, while a pair of heterochiral Fermi arcs are totally reflected. Following a Landauer approach (see SM [38] for details), the conductance is given by

$$G = n_{\text{ho}} N(B) \frac{e^2}{h}, \quad (1)$$

where  $n_{\text{ho}}$  is the number of homochiral Fermi arcs and  $N(B)$  is the number of incoming modes per unit area. Note that the conductance is independent of the occupation of higher Landau levels, which are perfectly reflected. This results in a universal conductance that is insensitive to material-specific details such as the energies of the Weyl nodes and velocities.

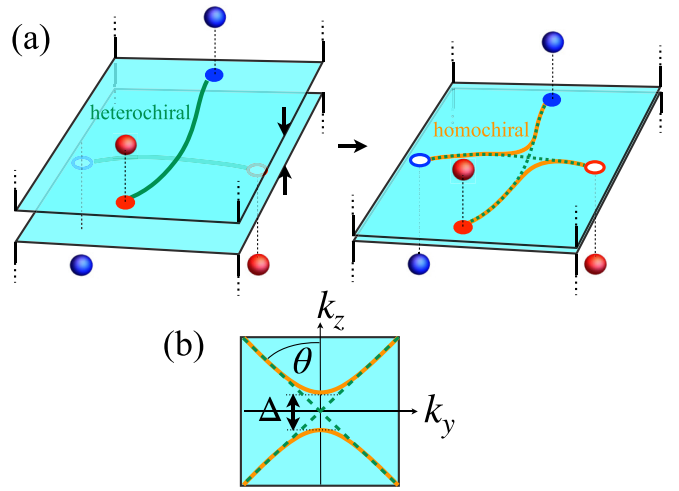


FIG. 2. (a) The interface of two WSMs with crossing Fermi arcs whose hybridization leads to a connectivity switch from heterochiral to homochiral. (b) The close encounter of interface Fermi arcs for a weak tunnel coupling.

*Magnetic breakdown.* The derivation of Eq. (1) breaks down once the magnetic field is large enough to enable backscattering via the interface Fermi arcs. This, however, only happens once  $\ell_B^{-1} \approx 0.004 \text{ \AA}^{-1} \sqrt{B[\text{T}]}$  (with  $B$  in Teslas) approaches the reciprocal space separation between the two chiral modes. Realistic magnetic fields can thus only couple modes whose separation is small compared to the size of the surface BZ, resulting in the phenomena of magnetic breakdown being considered rather exotic [27]. However, in our setup, a close encounter of interface Fermi arcs can be achieved by a weak tunnel coupling of two WSMs whose Fermi arcs cross in the decoupled limit, as illustrated in Fig. 2(a).

Near a close encounter of two Fermi arcs, the linearized interface Hamiltonian reads

$$H_{\text{int}}(\mathbf{k}_{\perp}) = (v_z \Delta / 2) \sigma_x + v_y k_y \sigma_z + v_z k_z, \quad (2)$$

where  $\mathbf{k}_{\perp}$  is the transverse momentum measured from the midpoint of the smallest separation between contours [see Fig. 2(b)], the Pauli matrices correspond to the two Fermi arcs from the decoupled system, the velocities  $v_y$  and  $v_z$  are fixed by the specific dispersion of the Fermi arcs, and  $\Delta$  quantifies the hybridization strength, which depends on the tunneling amplitude. The shortest distance between the Fermi arcs is then given by  $|\Delta|$  and  $\theta = \tan^{-1}(v_z/v_y)$  is half the angle of the Fermi arc intersection, as shown in Fig. 2(b).

The essential requirement for our setup is a crossing of interface Fermi arcs in the decoupled limit. At finite tunneling, such a crossing turns into a close encounter, unless protected by a symmetry deriving from the symmetries of the WSMs. Explicitly, this must forbid mass terms proportional to both  $\sigma_x$  and  $\sigma_y$  in Eq. (2). Such a protection, however, requires a lattice symmetry; which, though it may hold for interfaces between a pair of highly symmetric Weyl node configurations, would not hold for generic interfaces. The close encounter described above is thus generic so long as the decoupled Fermi arcs exhibit a crossing.

At a finite but small  $\Delta$ , a longitudinal magnetic field  $B$  enables quantum tunneling between the two Fermi arcs when  $\ell_B^{-1} \gtrsim \Delta$ . To quantify this magnetic breakdown, we deploy an analytical description following the standard formalism of Refs. [25,27,28,39]. Using the semiclassical wavefunctions of the Fermi arcs away from the encounter as scattering states that move along the arcs in accordance with the Lorentz force, we calculate the transition probability across the gap by matching the scattering states with the exact solutions of  $H_{\text{int}}$ . The resulting probability of tunneling between the arcs is given by [40]

$$P = e^{-B_0/B}, \quad B_0 = \frac{\pi}{4} \Delta^2 |\tan \theta|. \quad (3)$$

A particle passing a single encounter thus experiences a heterochiral connectivity—and is therefore reflected—with probability  $P$ , so that the probability of transmission across the interface is given by  $1 - P$ . The conductance is thus obtained by weighing Eq. (1) by a factor of  $1 - P$ , so that

$$G = N(B) \frac{e^2}{h} \sum_{i=1}^{n_{\text{ho}}} (1 - e^{-B_{0,i}/B}), \quad (4)$$

where the sum runs over all homochiral connectivities and  $B_{0,i}$  are the corresponding breakdown fields. For  $B \ll B_{0,i}$ , Eq. (1) is recovered, while for  $B \gg B_{0,i}$ , the conductance saturates at  $(e^2/h)N(B_{0,i})$ . In the latter limit, the transmission probability approaches zero as  $1/B$  (rendering the connectivity effectively heterochiral) but as  $N(B)$  is linear in  $B$ , the conductance saturates to a constant value.

If we further increase the magnetic field, it couples Weyl nodes of the same chirality on opposite sides of the interface. In this case, the modes can transmit across the interface directly (skipping the Fermi arc) so the transmission is no longer bounded from above by  $N(B)$ . The conductance then becomes nonuniversal: it depends on the number of occupied Landau levels. If the field is strong enough to couple opposite chirality nodes, then the WSM phase is effectively destroyed [41].

*Lattice simulation.* We test the above predictions by numerical and semianalytical calculations on a WSM lattice model. We consider Hamiltonians of the form [42]

$$\mathcal{H}(\mathbf{k}) = \mathcal{H}_x(k_x) + \eta_y(\mathbf{k}_\perp) \tau^y + \eta_z(\mathbf{k}_\perp) \tau^z, \quad (5)$$

where  $\mathcal{H}_x(k_x) = \sin k_x \tau^x + (1 - \cos k_x) \tau^z$  and the Pauli matrices  $\tau^a$  represent a pseudospin degree of freedom. The hopping strength along  $x$  and the lattice constant are set to one, and  $\eta_{y,z}(\mathbf{k}_\perp)$  are functions of the transverse momentum  $\mathbf{k}_\perp \equiv (k_y, k_z)$ . For  $\eta_z(\mathbf{k}_\perp) > -2$ , the model hosts Weyl nodes in the  $k_x = 0$  plane at  $\mathbf{k}_\perp$  satisfying  $\eta_y(\mathbf{k}_\perp) = \eta_z(\mathbf{k}_\perp) = 0$ . At a boundary normal to  $x$ , the Fermi arcs lie along  $\eta_y(\mathbf{k}_\perp) = 0$  for  $\eta_z(\mathbf{k}_\perp) < 0$  [42].

We consider an interface between two WSMs with

$$\begin{aligned} \eta_y^\pm(\mathbf{k}_\perp) &= \frac{1}{\sin b} [\pm \sin b_z \sin k_y + \sin b_y \sin k_z], \\ \eta_z^\pm(\mathbf{k}_\perp) &= \cos b_y + \cos b_z - \cos k_y - \cos k_z, \end{aligned} \quad (6)$$

where the superscript  $\pm$  refers to the left/right WSM. The corresponding Weyl nodes with chirality  $\chi$  lie at  $\mathbf{k}_\perp = \chi \mathbf{b}$ , where  $\mathbf{b} = (b_y, b_z) = b(\sin \tilde{\theta}, \cos \tilde{\theta})$ . The tunnel junction between these two WSMs is modelled by a reduced hopping

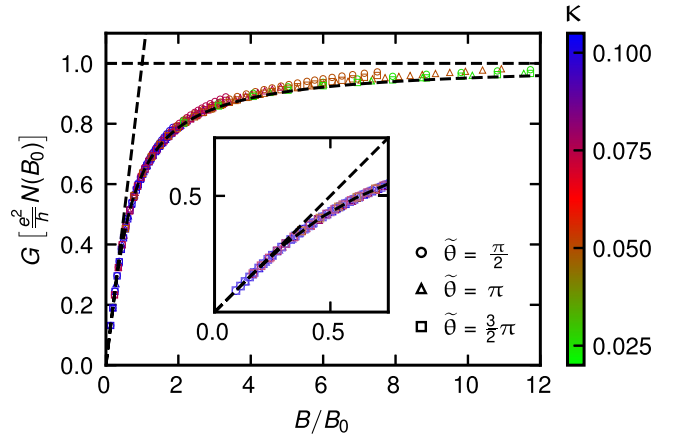


FIG. 3. Conductance, in units of the saturation value  $(e^2/h)N(B_0)$ , as a function of the magnetic field in units of the breakdown field  $B_0$ . The numerical computation is performed for model parameters  $b = \pi/2$ , energy  $E = 0.1$ , and various values of  $\theta$  and  $\kappa$ . The analytical result (black dashed curve) are in good agreement with the numerical results, with increasing deviations close to the field's upper bound (see below). The straight dashed lines indicate the predicted asymptotic low- and high-field behavior. For the numerical data, the upper bound on the magnetic field is set by the smallest magnetic length  $\ell_B = 3.1$  lattice units—since smaller  $\ell_B$  results in a trivial breakdown of WSM physics—while the lower bound is set to 13.8 lattice units. Data points corresponding to a smaller (larger) breakdown field  $B_0$  [for smaller (larger)  $\kappa$ ] thus span a range of fields at higher (lower) values of  $B/B_0$ . The inset shows a close-up at small fields; highlighting the deviation from perfect transmission caused by the onset of magnetic breakdown.

$0 \leq \kappa \leq 1$  along  $x$  at the interface. The conductance for this lattice model for various values of  $\theta$ , computed numerically using the *Kwant* package [43], are plotted in Fig. 3.

To compare the numerical results to the analytics without any fitting parameters, we derive the breakdown field of Eq. (3) from the lattice model parameters. To this end, we need to determine the intersection angle  $\theta$  of the Fermi arcs in the decoupled limit ( $\kappa = 0$ ) as well as the minimum separation  $\Delta$  between the hybridized ( $\kappa \neq 0$ ) Fermi arcs [cf. Fig. 2(b)]. The Fermi arcs in the decoupled limit are given by  $\eta_y^\pm(\mathbf{k}_\perp) = 0$ . Linearizing  $\eta_y^\pm$  around  $\mathbf{k}_\perp = 0$ , we get

$$\tan \theta = \frac{\sin b_y}{\sin b_z} = \frac{\sin(b \sin \tilde{\theta})}{\sin(b \cos \tilde{\theta})}. \quad (7)$$

We next derive the interface Fermi arcs at a finite coupling  $\kappa$  using a transfer-matrix approach [42,44], as described in the SM [38]. To leading order in  $\kappa \ll 1$ , the minimum separation is given by

$$\Delta = 2\kappa\beta(2 + \beta) \frac{\sin b}{\sin b_z}, \quad (8)$$

where  $\beta = \cos b_y + \cos b_z - 2$ . The breakdown field can then be determined by Eqs. (3), (7), and (8). The conductance computed using (4), with the analytically computed breakdown field, shows excellent agreement with the numerical results so long as the magnetic length is much larger than the lattice spacing, as shown in Fig. 3.

*Discussion and conclusions.* In this article, we consider magnetoconductance across a tunnel barrier between two WSMs arranged such that the projection of their Weyl node's Fermi surfaces onto the interface BZ are well separated and thereby not coupled by a magnetic field. At generic tunnel coupling, the interface Fermi arcs, which come in two topologically distinct connectivity types (heterochiral and homochiral), will typically also be well separated. In this regime, the system displays a universal tunnel magnetoconductance of  $(e^2/h)N(B)$  [where  $N(B)$  is the number of flux quanta through the interface] for each pair of homochiral-connectivity Fermi arcs. While the CME of a bulk WSM in the ballistic limit is also characterised by a universal magnetoconductance, where the number of homochiral Fermi-arc pairs is replaced by the number of Weyl-node pairs, it requires a minimal magnetic-field strength whose scale is set by the energy of the Weyl nodes and by diffusion properties [9,17]. Similarly nonuniversal is the conductance across interfaces with overlapping projections of Weyl Fermi pockets [20–23,35].

In contrast, the tunnel conductance considered here is independent of such details because the interface behaves as a filter, each Fermi arc transmitting exactly one  $N(B)$ -degenerate mode, while additional modes are reflected. A bulk system that displays a similar extension of the ballistic-limit CME down to zero magnetic field, independent of system details, is the Fermi-arc metal [45], recently predicted by Brouwer and one of us.

We have also shown that such interfaces can be used to realize the rare phenomena of magnetic breakdown. This requires a close encounter of two Fermi arcs so as to enable magnetic-field-induced quantum tunneling between them. Such an encounter is generic between WSMs whose interface Fermi arcs cross in the decoupled limit. The magnetic breakdown leads to a suppression of the transmission probability for field strengths above a characteristic breakdown field  $B_0$  (set by the coupling strength). Since magnetic breakdown effectively turns a homochiral connectivity into a heterochiral one, one might expect the conductance to drop to zero above  $B_0$ . The increased probability of experiencing a heterochiral connectivity at higher fields is, however, balanced by the increased degeneracy of transmitted modes, leading to a saturation of the conductance at a finite value of  $(e^2/h)N(B_0)$ .

As for material realizations of the tunnel-junction CME, one could use WSM interfaces, for which the separation between projections of Fermi pockets from opposite sides of the interface is larger than the inverse magnetic length. The inverse magnetic length (at realistic magnetic field strengths) and the size of Fermi-pocket projections in many existing WSMs are sufficiently small to realize an interface without an overlap of bulk states. Otherwise, overlapping bulk states will produce additional conducting channels that will add to the universal Fermi-arc conductance. Moreover, the universal tunnel conductance is robust with respect to the presence of additional, nontopological surface states since it only depends on the Fermi-arc connectivity, which is robust against hybridization with other surface states. The presence of surface disorder and phonons could modify the transmission behavior by introducing scattering between counterpropagating states separated in the in-plane momentum. For weak disorder and low temperatures this effect is of subleading order in the corresponding scattering amplitude and becomes negligible for long-ranged potentials and well-separated Fermi arcs since counterpropagating states are then not continuously connected [46]. For material realizations of the magnetic-breakdown effect, one could use a tunnel junction between identical WSMs rotated with respect to one another by a small angle. Materials with curved Fermi arcs, such as those of the TaAs and RhSi families, will then typically host Fermi arc crossings (in the decoupled limit) for which a weak tunnel coupling would lead to a close encounter.

A possible future avenue would be to harness the magnetic-breakdown induced splitting of quasiparticle trajectories to enable interference between different interface trajectories. Such interference effects have a rich history of providing experimental access to the Fermiology of bulk materials [29,47–50]; the magnetic breakdown of interface Fermi arcs that we predict may play a similar role in the Fermiology of Fermi-arc surface states.

*Acknowledgments.* We thank Piet W. Brouwer, Haoyang Tian, Achim Rosch, Reinhold Egger, and Francesco Buccheri for useful discussions. This research was supported by Projects A02 and A03 of the CRC-TR 183 “Entangled States of Matter” and Grant No. 18688556 of the Deutsche Forschungsgemeinschaft (DFG, German Science Foundation).

- 
- [1] X. Wan, A. M. Turner, A. Vishwanath, and S. Y. Savrasov, Topological semimetal and Fermi-arc surface states in the electronic structure of pyrochlore iridates, *Phys. Rev. B* **83**, 205101 (2011).
- [2] A. A. Burkov and L. Balents, Weyl Semimetal in a Topological Insulator Multilayer, *Phys. Rev. Lett.* **107**, 127205 (2011).
- [3] G. Xu, H. Weng, Z. Wang, X. Dai, and Z. Fang, Chern Semimetal and the Quantized Anomalous Hall Effect in  $\text{HgCr}_2\text{Se}_4$ , *Phys. Rev. Lett.* **107**, 186806 (2011).
- [4] S.-Y. Xu, C. Liu, S. K. Kushwaha, R. Sankar, J. W. Krizan, I. Belopolski, M. Neupane, G. Bian, N. Alidoust, T.-R. Chang *et al.*, Observation of Fermi arc surface states in a topological metal, *Science* **347**, 294 (2015).
- [5] S.-Y. Xu, N. Alidoust, I. Belopolski, Z. Yuan, G. Bian, T.-R. Chang, H. Zheng, V. N. Strocov, D. S. Sanchez, G. Chang *et al.*, Discovery of a Weyl fermion state with Fermi arcs in niobium arsenide, *Nat. Phys.* **11**, 748 (2015).
- [6] B. Q. Lv, H. M. Weng, B. B. Fu, X. P. Wang, H. Miao, J. Ma, P. Richard, X. C. Huang, L. X. Zhao, G. F. Chen, Z. Fang, X. Dai, T. Qian, and H. Ding, Experimental Discovery of Weyl Semimetal TaAs, *Phys. Rev. X* **5**, 031013 (2015).
- [7] N. P. Armitage, E. J. Mele, and A. Vishwanath, Weyl and Dirac semimetals in three dimensional solids, *Rev. Mod. Phys.* **90**, 015001 (2018).
- [8] B. Yan and C. Felser, Topological materials: Weyl semimetals, *Annu. Rev. Condens. Matter Phys.* **8**, 337 (2017).

- [9] A. A. Burkov, Weyl metals, *Annu. Rev. Condens. Matter Phys.* **9**, 359 (2018).
- [10] M. Z. Hasan, G. Chang, I. Belopolski, G. Bian, S. Y. Xu, and J. X. Yin, Weyl, Dirac and high-fold chiral fermions in topological quantum matter, *Nat. Rev. Mater.* **6**, 784 (2021).
- [11] B. A. Bernevig, C. Felser, and H. Beidenkopf, Progress and prospects in magnetic topological materials, *Nature (London)* **603**, 41 (2022).
- [12] S. L. Adler, Axial-vector vertex in spinor electrodynamics, *Phys. Rev.* **177**, 2426 (1969).
- [13] J. S. Bell and R. W. Jackiw, A PCAC puzzle:  $\pi^0 \rightarrow \gamma\gamma$  in the  $\sigma$ -model, *Nuov Cim. A* **60**, 47 (1969).
- [14] H. B. Nielsen and M. Ninomiya, The Adler-Bell-Jackiw anomaly and Weyl fermions in a crystal, *Phys. Lett. B* **130**, 389 (1983).
- [15] D. T. Son and B. Z. Spivak, Chiral anomaly and classical negative magnetoresistance of Weyl metals, *Phys. Rev. B* **88**, 104412 (2013).
- [16] J. Xiong, S. K. Kushwaha, T. Liang, J. W. Krizan, M. Hirschberger, W. Wang, R. J. Cava, and N. P. Ong, Evidence for the chiral anomaly in the Dirac semimetal  $\text{Na}_3\text{Bi}$ , *Science* **350**, 413 (2015).
- [17] A. Altland and D. Bagrets, Theory of the strongly disordered Weyl semimetal, *Phys. Rev. B* **93**, 075113 (2016).
- [18] R. D. dos Reis, M. O. Ajeesh, N. Kumar, F. Arnold, C. Shekhar, M. Naumann, M. Schmidt, M. Nicklas, and E. Hassinger, On the search for the chiral anomaly in Weyl semimetals: The negative longitudinal magnetoresistance, *New J. Phys.* **18**, 085006 (2016).
- [19] B. Q. Lv, T. Qian, and H. Ding, Experimental perspective on three-dimensional topological semimetals, *Rev. Mod. Phys.* **93**, 025002 (2021).
- [20] K. Kobayashi, Y. Ominato, and K. Nomura, Helicity-protected domain-wall magnetoresistance in ferromagnetic Weyl semimetal, *J. Phys. Soc. Jpn.* **87**, 073707 (2018).
- [21] D. J. P. de Sousa, C. O. Ascencio, P. M. Haney, J. P. Wang, and T. Low, Gigantic tunneling magnetoresistance in magnetic Weyl semimetal tunnel junctions, *Phys. Rev. B* **104**, L041401 (2021).
- [22] S. Tchoumakov, B. Bujnowski, J. Noky, J. Gooth, A. G. Grushin, and J. Cayssol, Conservation of chirality at a junction between two Weyl semimetals, *Phys. Rev. B* **104**, 125308 (2021).
- [23] F. Bucchieri, R. Egger, and A. De Martino, Transport, refraction, and interface arcs in junctions of Weyl semimetals, *Phys. Rev. B* **106**, 045413 (2022).
- [24] N. A. Lanzillo, U. Bajpai, I. Garate, and C. T. Chen, Size-Dependent Grain-Boundary Scattering in Topological Semimetals, *Phys. Rev. Appl.* **18**, 034053 (2022).
- [25] M. H. Cohen and L. M. Falicov, Magnetic Breakdown in Crystals, *Phys. Rev. Lett.* **7**, 231 (1961).
- [26] E. I. Blount, Bloch electrons in a magnetic field, *Phys. Rev.* **126**, 1636 (1962).
- [27] D. Shoenberg, *Magnetic Oscillations in Metals*, Cambridge Monographs on Physics (Cambridge University Press, Cambridge, 1984).
- [28] M. I. Kaganov and A. A. Slutskin, Coherent magnetic breakdown, *Phys. Rep.* **98**, 189 (1983).
- [29] M. R. van Delft, S. Pezzini, T. Khouri, C. S. A. Müller, M. Breitzkreiz, L. M. Schoop, A. Carrington, N. E. Hussey, and S. Wiedmann, Electron-Hole Tunneling Revealed by Quantum Oscillations in the Nodal-Line Semimetal  $\text{HfSiS}$ , *Phys. Rev. Lett.* **121**, 256602 (2018).
- [30] S. E. Sebastian, N. Harrison, R. Liang, D. A. Bonn, W. N. Hardy, C. H. Mielke, and G. G. Lonzarich, Quantum Oscillations from Nodal Bilayer Magnetic Breakdown in the Underdoped High Temperature Superconductor  $\text{YBa}_2\text{Cu}_3\text{O}_{6+x}$ , *Phys. Rev. Lett.* **108**, 196403 (2012).
- [31] In the case of Weyl nodes with a topological charge greater than one or the case of overlapping Weyl node projections from the same WSM,  $N(B)$  is multiplied by the absolute value of the total topological charge at the Weyl-node projection.
- [32] V. Dwivedi, Fermi arc reconstruction at junctions between Weyl semimetals, *Phys. Rev. B* **97**, 064201 (2018).
- [33] F. Abdulla, S. Rao, and G. Murthy, Fermi arc reconstruction at the interface of twisted Weyl semimetals, *Phys. Rev. B* **103**, 235308 (2021).
- [34] N. Mathur, F. Yuan, G. Cheng, S. Kaushik, I. Robredo, M. G. Vergniory, J. Cano, N. Yao, S. Jin, and L. M. Schoop, Atomically sharp internal interface in a chiral Weyl semimetal nanowire, *Nano Lett.* **23**, 2695 (2023).
- [35] S. Kaushik, I. Robredo, N. Mathur, L. M. Schoop, S. Jin, M. G. Vergniory, and J. Cano, Transport signatures of Fermi arcs at twin boundaries in Weyl materials, [arXiv:2207.14109](https://arxiv.org/abs/2207.14109).
- [36] G. Murthy, H. A. Fertig, and E. Shimshoni, Surface states and arcless angles in twisted Weyl semimetals, *Phys. Rev. Res.* **2**, 013367 (2020).
- [37] R. Kundu, H. A. Fertig, and A. Kundu, Broken symmetry and competing orders in Weyl semimetal interfaces, *Phys. Rev. B* **107**, L041402 (2023).
- [38] See Supplemental Material at <http://link.aps.org/supplemental/10.1103/PhysRevB.107.L241109> for a topological explanation of interface Fermi arcs, details on the interface conductance derivation, and details of the lattice simulation.
- [39] L. D. Landau and E. M. Lifshitz, *Course of Theoretical Physics* (Elsevier, Oxford, 1977).
- [40] M. Breitzkreiz, N. Bovenzi, and J. Tworzydło, Phase shift of cyclotron orbits at type-I and type-II multi-Weyl nodes, *Phys. Rev. B* **98**, 121403(R) (2018).
- [41] B. J. Ramshaw, K. A. Modic, A. Shekhter, Y. Zhang, E.-A. Kim, P. J. W. Moll, M. D. Bachmann, M. K. Chan, J. B. Betts, F. Balakirev *et al.*, Quantum limit transport and destruction of the Weyl nodes in TaAs, *Nat. Commun.* **9**, 2217 (2018).
- [42] V. Dwivedi and V. Chua, Of bulk and boundaries: Generalized transfer matrices for tight-binding models, *Phys. Rev. B* **93**, 134304 (2016).
- [43] C. W. Groth, M. Wimmer, A. R. Akhmerov, and X. Waintal, Kwant: A software package for quantum transport, *New J. Phys.* **16**, 063065 (2014).
- [44] V. Dwivedi and S. T. Ramamurthy, Connecting the dots: Time-reversal symmetric Weyl semimetals with tunable Fermi arcs, *Phys. Rev. B* **94**, 245143 (2016).
- [45] M. Breitzkreiz and P. W. Brouwer, Fermi-Arc Metals, *Phys. Rev. Lett.* **130**, 196602 (2023).
- [46] P. M. Perez-Piskunow, N. Bovenzi, A. R. Akhmerov, and M. Breitzkreiz, Chiral anomaly trapped in Weyl metals: Nonequilibrium valley polarization at zero magnetic field, *SciPost Phys.* **11**, 046 (2021).

- [47] L. M. Falicov and H. Stachowiak, Theory of the de Haas-van Alphen effect in a system of coupled orbits. Application to magnesium, *Phys. Rev.* **147**, 505 (1966).
- [48] R. W. Stark and R. Reifenberger, Quantitative theory for the quantum interference effect in the transverse magnetoresistance of pure magnesium, *J. Low Temp. Phys.* **26**, 763 (1977).
- [49] C. Albrecht, J. H. Smet, D. Weiss, K. von Klitzing, R. Hennig, M. Langenbuch, M. Suhrke, U. Rössler, V. Umansky, and H. Schweizer, Fermiology of Two-Dimensional Lateral Superlattices, *Phys. Rev. Lett.* **83**, 2234 (1999).
- [50] A. Alexandradinata and L. Glazman, Fermiology of topological metals, *Annu. Rev. Condens. Matter Phys.* **14**, 261 (2023).